STRUCTURAL PROPERTIES OF THE LOCAL GALAXY POPULATION

Paul D. Allen
Mount Stromlo Observatory, The Australian National University

Abstract. The Millennium Galaxy Catalogue is a deep, wide imaging and redshift survey that provides a representative and complete sample of galaxies in the local Universe. GIM2D is used to model the light profiles for over 10000 resolved MGC galaxies. Three different schemes are used: (1) $R^{1/4}$+Exponential; (2) $R^{1/n}$+Exponential; (3) $R^{1/n}$. With careful quality control the resulting catalogues are shown to be robust for those galaxies with component half-light radii greater than the seeing, providing a valuable resource for measuring fundamental galaxy parameters for comparison with both theory, and measurements at high redshift.

1 Introduction

Even at $z \sim 1$, the dominant structural features in the majority of galaxies appear to be bulges and disks [23, 21, 4, 16, 26]. Models of galaxy formation and evolution generally involve separate formation scenarios for bulges and disks (e.g. Cole et al., 2000; Kormendy & Kennicutt 2004)[6, 17], and they are often observed to have different average colours, metallicities, and kinematics, justifying their treatment as distinct entities. Within the ΛCDM paradigm, it is possible to make specific predictions relating the mass and angular momentum of dark matter haloes with the observed distributions in galaxy luminosity and size as a function of redshift (e.g. Mo, Mao, & White 1998, Bouwens & Silk 2004)[19, 5]. It is desirable to describe galaxies in terms of the 2-component bulge-disk model at different epochs to not only constrain these models, but also to explain the distributions that are observed in the galaxy population today. Therefore, bulge-disk decomposition is a popular and useful method for quantifying the morphologies of galaxies by fitting model surface brightness profiles to data.

A bulge-disk model is also convenient because the surface brightness profiles of bulges can be modelled by an $R^{1/4}$ law [11], an exponential profile [3, 9], or more optimally using a Sérsic profile [22, 15], and disks are observed to follow exponential laws [12, 14]. Finally, software is now available which makes it a fairly straightforward task to perform bulge-disk decomposition on many thousands of galaxies [24, 20, 25, 10].

Here, we discuss the use of one such publically available bulge-disk decomposition code, GIM2D [24], to provide a quantitative measure of the surface brightness profiles of 10095 galaxies in the Millennium Galaxy Catalogue (MGC). This provides a catalogue of structural measurements for a representative and complete sample of galaxies in the ($z \sim 0$) local Universe.

2 The Millennium Galaxy Catalogue

The Millennium Galaxy Catalogue[1] (MGC) is a deep (μ_{lim}=26 B mags/arcsec^2), wide area ($\sim$37.5 deg^2) imaging and redshift survey covering a 0.5 deg wide strip along the equatorial sky from 10h to 14h50$'$. The imaging was carried out using the INT Wide Field Camera (WFC). The survey region overlaps both the 2dFGRS [7], and SDSS-DR1 [1], providing both $u'g'r'i'z'$ photometry, and redshifts for 47.0% of the 10095 resolved galaxies with $B < 20$ mag. The remaining $B < 20$ galaxies without known redshifts were observed as targets in the spectroscopic part of the survey, MGCz. This mostly involved observations using the 2dF instrument on the AAT providing redshifts for a further 47.2% of galaxies in the sample. However, in order to avoid significant redshift incompleteness for objects with low surface brightness [13], both 4-m (ESO/NTT and TNG) and 8-m (Gemini) observations were carried out to obtain spectra for the lowest surface brightness galaxies in the sample.

Comparison between 2dFGRS, SDSS and the MGC shows that the MGC is deeper, more complete, more precise, and of higher spatial resolution than either the 2dFGRS or SDSS-DR1 data sets [8, 13]. The increased depth and resolution is demonstrated in Figure 1. Full details of the MGC, including observations, data reduction, image detection and classification, are given in Liske et al. (2003). The MGC redshift survey is discussed in detail in Driver et al. (2005).

With a photometric precision of 0.03 mag, astrometric accuracy of 0.08 arcsec [18], and 96% redshift completeness to $B_{\rm MGC} = 20$ mag (increasing to 99.8% for $B_{\rm MGC} < 19.2$ mag), the MGC represents an extremely high quality and high completeness census of the nearby galaxy population. It is therefore the ideal data set to

[1]The MGC is publically available at http://www.eso.org/ ~jliske/mgc

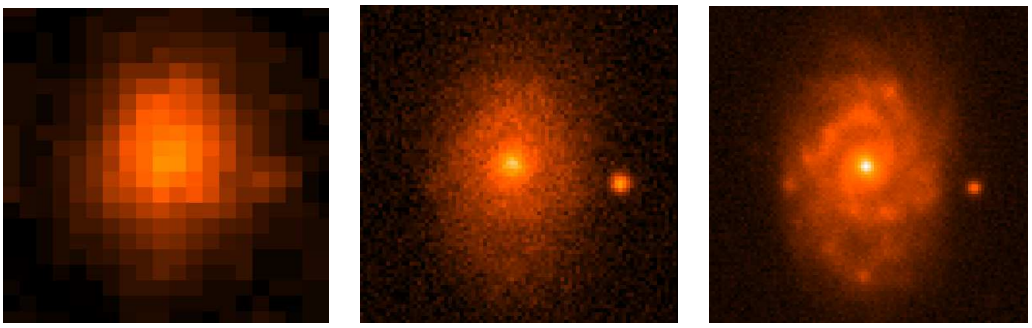

Figure 1: A comparison between Digitized Sky Survey (left, b_J-band), SDSS-DR1 (centre, g-band), and the MGC (right), for MGC04795

use for a detailed analysis of the structural composition of galaxies in the local Universe, and to provide a low redshift anchor for higher redshift studies.

3 Using GIM2D to model Galaxy Light Profiles

In Allen et al., (2005) [2] the 2-D light profiles for all 10095 MGC galaxy images were modelled using the GIM2D package [24]. GIM2D allows galaxies to be modelled using a single component model, or a two component model with separate profiles for the bulge and disk components. For the MGC, three schemes were used:

- Sérsic – single component.
- De Vaucouleurs Bulge + Exponential Disk.
- Sérsic Bulge + Exponential Disk.

It is important to separate the intrinsic morphologies of galaxies from distortions that arise from the combined optical system of telescope, instrument, and atmosphere. Therefore the point spread function (PSF) was also modelled for each galaxy using stars that lie in the same frame as the galaxy. GIM2D then finds the best-fitting PSF-convolved model for each galaxy using the pixels designated as part of the object by the SEXtractor segmentation image mask (see [24]). This resulted in three structural catalogues containing measurements of total flux, bulge to disk flux ratio (B/T), and the $x-y$ position of the central surface brightness. For bulges, effective radii (R_e), Sérsic index (n), ellipticity (ϵ), and position angle (ϕ_b) are all measured. For disks, the catalogues contain measurements of scale-length (h), inclination (i), and disk position angle (ϕ_d). Figure 2 shows example output and residual images for the galaxy MGC27301 along with the raw image, mask, PSF, and a plot of the best-fitting model for this galaxy using the Sérsic+Exponential fit.

3.1 Quality Control

As an initial test of the accuracy of the GIM2D output, simple global observables such as magnitudes, half-light radii, and $x-y$ centroid positions can be compared to the values measured by other means in Liske et al. (2003). For example, differences between GIM2D output and previous measurements can be indicative of bad SExtractor segmentation images. If a galaxy has been over-deblended, then the GIM2D magnitude will be an under-estimate. When two nearby galaxies are treated as one, the centroids will be grossly different, and the GIM2D magnitudes over-estimated. It was found that 222 segmentation images needed to be corrected. No restrictions on the relative sizes of 'bulge' and 'disk' components are applied by GIM2D. The two components can sometimes be inverted or used to fit other structural features, especially in irregular galaxies. It is therefore important to ensure that the fits are interpreted correctly (see [2]).

Due to overlaps between pointings of the WFC, 702 objects had duplicate observations. In many cases the observations were carried out on a different night or even as part of different observing runs several months apart. They therefore provide an excellent test of the repeatability of GIM2D fits for a diverse and representative sample of galaxies under different conditions. For each parameter we compute the mean residual between repeat measurements and the $3-\sigma$ clipped standard deviation. In all cases the mean is close to zero. However, the comparison reveals that if the half light radius of a component is sufficiently large ($R_e > 0.8\Gamma$ or $1.678h > 0.8\Gamma$

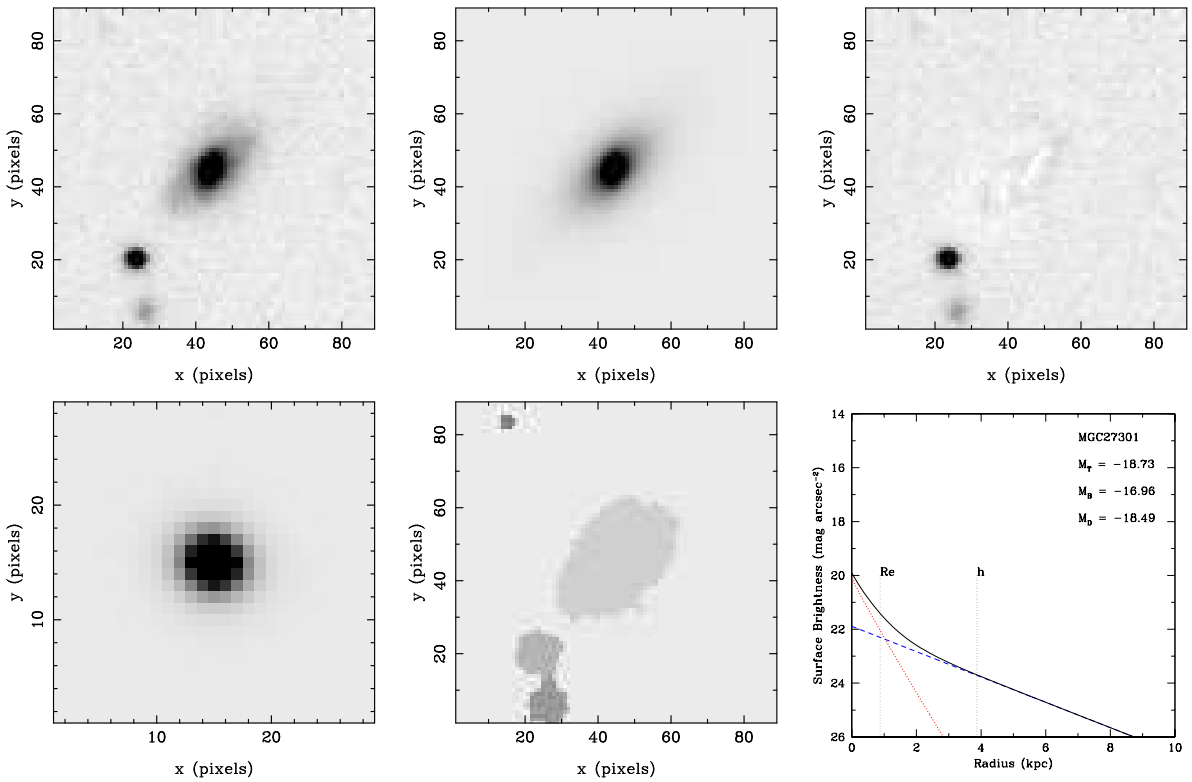

Figure 2: GIM2D input and output for the galaxy MGC27301. The output model shown is for the Sérsic+Exponential fit. The top row shows images of the galaxy (left), the GIM2D model image (centre), and the residual image showing the difference. The bottom row shows the input PSF (left), the segmentation image or mask (centre). The bottom right panel shows the best-fitting profile. The dashed straight line represents the exponential (disk) component, and the dotted curve corresponds to the Sérsic(bulge) component. The total profile is shown by the solid bold curve. R_e and h are also shown.

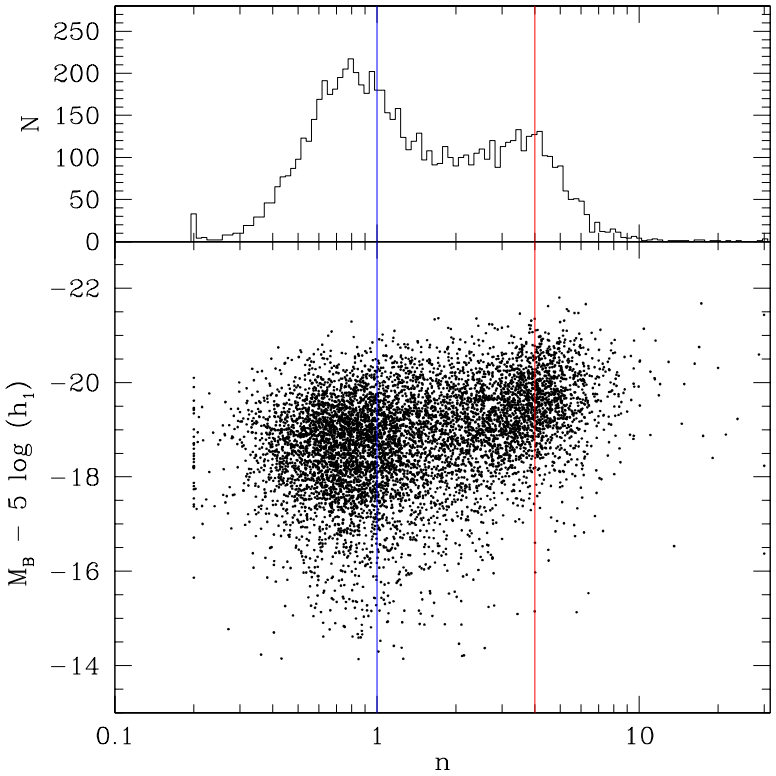

Figure 3: (upper) The histogram of recovered Sérsic index from the Sérsic only profile fits. (lower) The distribution of Sérsic versus absolute magnitude.

where Γ is the seeing FWHM), then for the Sérsic+Exponential model the standard deviations between repeat measurements are: $R_e \sim 13.2\%$, $\log(n) \sim 13.6\%$, and $h \sim 6\%$. For the component magnitudes: $M_{bulge} \sim 0.24$ mags, and $M_{disk} \sim 0.14$ mags. For single component Sérsic models the standard deviations are $R_e = 4\%$, $\epsilon = 0.02$, $M = 0.04$ mags, and $\log(n) = 0.04$.

4 Conclusions

The Millennium Galaxy Catalogue is a deep, wide survey of the local galaxy population, and its completeness, depth and resolution make it ideal for the provision of a representative sample of galaxy structural measurements at $z \sim 0$. GIM2D has been used to obtain the best-fitting Sérsic models, Sérsic+Exponential decompositions, and de Vaucouleurs+Exponential decompositions to the 100095 galaxies with $B < 20$ in the MGC. The resulting structural catalogues are made publically available in Allen et al. (2005). With careful quality control, repeatable measurements are obtainable for galaxy components that are larger than the seeing FWHM for both two component, and single component fits. Although the principal aim of this work is to treat bulges and disks separately, the existence of bulge and disk dominated systems is evident even in the single Sérsic component fits. Figure 3 (upper) shows the distribution of the $\log(n)$ from the Sérsic profile only catalogue. A bimodal distribution is clearly evident. The vertical lines show the $n = 1$ (i.e., pure exponential) and $n = 4$ (i.e., de Vaucouleurs profile). The two peaks lie at approximately $n = 0.8$ and $n = 4$ and the obvious association is between disk-dominated systems and spheroids with a connection of bulge+disk systems. The lower panel of Figure 3 shows the relationship between Sérsic index, n, and absolute magnitude. It is clear that high-n, bulge dominated systems tend to be brighter.

The measured parameters from these catalogues can then be used to measure luminosity functions and bivariate brightness distributions for the separate populations (see Liske *these proceedings*), and by using bulge sersic indices, to measure the mass function for supermassive black holes at $z \sim 0$ (see Driver *these proceedings*).

References

[1] Abazajian, K., et al. (2003). AJ, 126:2081–2086.

[2] Allen, P. D., Driver, S. P., Liske, J., Graham, A., Cameron, E., Cross, N. J. G., and de Propris, R. (2005). MNRAS, submitted.

[3] Andredakis, Y. C. and Sanders, R. H. (1994). MNRAS, 267:283–296.

[4] Barden, M., et al. (2005). astro-ph/0502416.

[5] Bouwens, R. and Silk, J. (2002). ApJ, 568:522–538.

[6] Cole, S., Lacey, C. G., Baugh, C. M., and Frenk, C. S. (2000). MNRAS, 319:168–204.

[7] Colless, M., et al (2001). MNRAS, 328:1039–1063.

[8] Cross, N. J. G., Driver, S. P., Liske, J., Lemon, D. J., Peacock, J. A., Cole, S., Norberg, P., and Sutherland, W. J. (2004). MNRAS, 349:576–594.

[9] de Jong, R. S. (1996). A&AS, 118:557–573.

[10] de Souza, R. E., Gadotti, D. A., and dos Anjos, S. (2004). ApJS, 153:411–427.

[11] de Vaucouleurs, G. (1948). *Annales d'Astrophysique*, 11:247.

[12] de Vaucouleurs, G. (1959). *Handbuch der Physik*, 53:275.

[13] Driver, S. P., Liske, J., Cross, N. J. G., De Propris, R., and Allen, P. D. (2005). MNRAS, 360:81–103.

[14] Freeman, K. C. (1970). ApJ, 160:811.

[15] Graham, A. W. and Driver, S. P. (2005). *PASA*, 22:118.

[16] Koo, D. C., et al (2005). ApJS, 157:175–217.

[17] Kormendy, J. and Kennicutt, R. C. (2004). ARA&A, 42:603–683.

[18] Liske, J., Lemon, D. J., Driver, S. P., Cross, N. J. G., and Couch, W. J. (2003). MNRAS, 344:307–324.

[19] Mo, H. J., Mao, S., and White, S. D. M. (1998). MNRAS, 295:319–336.

[20] Peng, C. Y., Ho, L. C., Impey, C. D., and Rix, H. (2002). AJ, 124:266–293.

[21] Ravindranath, S., et al (2004). ApJ, 604:L9–L12.

[22] Sersic, J. L. (1968). *Atlas de galaxias australes*. Cordoba, Argentina: Observatorio Astronomico, 1968.

[23] Simard, L., et al (1999). ApJ, 519:563–579.

[24] Simard, L., et al (2002). ApJS, 142:1–33.

[25] Trujillo, I. and Aguerri, J. A. L. (2004). MNRAS, 355:82–96.

[26] Trujillo, I., et al (2005). astro-ph/0504225.